



## Supporting Online Material for

### **Simultaneously Mitigating Near-Term Climate Change and Improving Human Health and Food Security**

Drew Shindell,\* Johan C. I. Kuylenstierna, Elisabetta Vignati, Rita van Dingenen, Markus Amann, Zbigniew Klimont, Susan C. Anenberg, Nicholas Muller, Greet Janssens-Maenhout, Frank Raes, Joel Schwartz, Greg Faluvegi, Luca Pozzoli, Kaarle Kupiainen, Lena Höglund-Isaksson, Lisa Emberson, David Streets, V. Ramanathan, Kevin Hicks, N. T. Kim Oanh, George Milly, Martin Williams, Volodymyr Demkine, David Fowler

\*To whom correspondence should be addressed. E-mail: [drew.t.shindell@nasa.gov](mailto:drew.t.shindell@nasa.gov)

Published 13 January 2012, *Science* **335**, 183 (2012)  
DOI: 10.1126/science.1210026

#### **This PDF file includes:**

Materials and Methods  
Figs. S1 to S6  
Tables S1 to S5  
References

## **Supporting Online Material for “Simultaneously mitigating near-term climate change and improving human health and food security”**

- Drew Shindell, Johan C. I. Kuylenstierna, Elisabetta Vignati, Rita van Dingenen, Markus Amann, Zbigniew Klimont, Susan C. Anenberg, Nicholas Muller, Greet Janssens-Maenhout, Frank Raes, Joel Schwartz, Greg Faluvegi, Luca Pozzoli, Kaarle Kupiainen, Lena Höglund-Isaksson, Lisa Emberson, David Streets, V. Ramanathan, Kevin Hicks, Kim Oanh, George Milly, Martin Williams, Volodymyr Demkine, David Fowler

### *Methodology:*

A series of modeling steps were carried out to analyze the effects of emissions control measures. These are schematically illustrated in Fig. S1, with details given in the sections below. Additional background on the methods used in the UNEP/WMO Integrated Assessment of Black Carbon and Tropospheric Ozone (1) can be found in chapters 4 and 5 of that work. This SOM draws on that material, written by the same authors, for sections where the methods overlap, though other sections such as the ‘Climate Simulations’ section are exclusive to this SOM.

### *Emissions:*

Emissions estimates were developed using the GAINS (Greenhouse gas – Air Pollution Interactions and Synergies) model, developed by the International Institute for Applied Systems Analysis (IIASA). This model is a successor to the RAINS model (2), incorporating the latest scientific understanding of air pollution, and has been extended to cover mitigation of greenhouse gases. GAINS brings together information on current and future economic, energy and agricultural development, emission control potentials and costs, atmospheric dispersion and environmental sensitivities towards air pollution (3). These impacts are considered in a multi-pollutant context, quantifying the contributions of SO<sub>2</sub>, NO<sub>x</sub>, NH<sub>3</sub>, NMVOC, and emissions of primary particulate matter, discriminating between fine and coarse particles as well as black carbon (BC) and organic carbon (OC). GAINS also accounts for emissions of the six greenhouse gases that are included in the Kyoto protocol, i.e., CO<sub>2</sub>, CH<sub>4</sub>, N<sub>2</sub>O, and the three F-gases. The GAINS model is implemented as an interactive web-based tool and is freely available over the Internet (<http://gains.iiasa.ac.at>).

The GAINS model has been applied to support international negotiations and discussion on the cost-effectiveness of alternative emission control strategies and distributional aspects of involved economic burdens and environmental benefits (e.g. (4-7)), including most recently climate and air quality policy co-benefits. In our current analysis, the application of GAINS has been limited to estimation of baseline emissions, analysis of abatement potential of measures addressing primarily short-lived climate forcers, and calculating a set of control scenarios applying a subset of selected measures. GAINS includes ~1650 measures with different individual impacts on emissions which can be grouped into ~400 broader categories of measures such as those used here (e.g. EUROVI on diesel cars, on light duty trucks, and on heavy duty trucks have distinct effects on emissions but can all be categorized as part of a diesel vehicle measure).

The fourteen specific measures identified by IIASA, using the net GWP reduction achieved as the sole selection criterion, are shown in Table S1, while the resulting emissions changes are shown in Figure S2. Though the 100-year GWP metric was chosen as the selection criterion for the measures, since CO<sub>2</sub> emissions were largely unaffected, and hence the compounds that were altered were all comparatively short-lived, using another time horizon such as 20 or 50 years would have little impact, as all GWP values would change similarly. We point out that the measures were not selected to be the ones that have the greatest impact on regional climate in any particular location, nor do they cause the greatest improvements in regional air quality. We also note that the relative cost of implementing the measures was not considered in the selection of measures, nor was the relative difficulty of implementation. Of course, the costs of implementing the measures were considered afterwards, as discussed in the main text. The feasibility of implementing the measures worldwide depends on society's motivation to do so, which will in part be governed by estimates of the measures' impacts such as those provided here. All the measures are inherently quite feasible to implement since they rely on existing, demonstrated technology (unlike the assumptions in many emissions scenarios). Finally, we point out that in the UNEP/WMO assessment, two additional BC measures were included in part of the analysis, but these are not addressed here, as these were not included in the global composition-climate modeling done by both groups. For both the reference case and the impacts of the measures, regional or national emission changes were mapped onto a worldwide grid using the spatial distribution by emission activity from the EDGAR database (8). Note that changes in methane emissions under the IEA's '450 CO<sub>2</sub>-equivalent' scenario were purposely not included so as to avoid double counting when creating the combined CO<sub>2</sub> plus methane and BC measures scenario. Thus the total warming mitigation achieved by the IEA 450 CO<sub>2</sub>-equivalent scenario would be somewhat greater than the CO<sub>2</sub> portion shown here. The impact of adding the IEA's methane measures on near-term climate is much less than that of the methane measures scenario examined here, however, as we consider both larger and more rapid methane emissions reductions. Note that within the combined oil and gas production sector, measures controlling emissions from oil production have about 5 times the global effect of measures on gas production.

- We assumed that emissions controls were implemented everywhere in the world to the maximum extent technology allows, in general. Hence they represent the maximum probable impact of those technologies. However, the measures do not encompass the full range of emissions reductions that could be achieved by large-scale societal changes such as shifting to electric vehicles (e.g. (9)). Nor do they encompass more fundamental changes such as from private vehicles to electrified public transportation, from trucks to electrified rail for cargo (in both cases assuming electricity is derived from clean sources), enhanced standards, for example fuel economy, or dramatically greater use of renewables rather than fossil fuels, including natural gas (e.g. (10)). Hence further work could usefully characterize the choices available to policy makers in particular regions based on these various other considerations aside from mitigation of global climate change through technical measures, and could quite reasonably come up with mitigation potential substantially larger than that found here.

#### *Composition-Climate Models:*

The GISS model for Physical Understanding of Composition-Climate Interactions and Impacts (GISS-PUCCINI) incorporates gas-phase (11), sulfate (12), black carbon (13), nitrate

(14) and secondary organic (15) aerosol chemistry within the GISS ModelE general circulation model (16). The chemistry scheme is quite similar to that documented previously, with the most notable additions being that acetone has been added to the hydrocarbons included in the model and a reaction pathway for  $\text{HO}_2 + \text{NO}$  to yield  $\text{HNO}_3$  has been added (17). The scheme now includes 156 chemical reactions among 50 species. Evaluations of the present-day composition in the model against observations are generally quite reasonable (as documented in the references given above as well as in, for example, (18, 19). The aerosol optical depths and radiative forcing per unit burden change in this model have been discussed and compared with other models and available satellite observations previously (18, 20, 21), with some additional evaluation for the current configuration in the UNEP/WMO Assessment.

For these simulations, we have used the development version of the model near its “frozen” state for AR5 simulations. The model has a horizontal resolution of  $2^\circ$  latitude by  $2.5^\circ$  longitude, with increased effective resolution for tracers due to carrying higher order moments at each grid box. This configuration had 40 vertical hybrid sigma layers from the surface to 0.1 hPa. Tracer transport uses a non-diffusive quadratic upstream scheme (22). Prescribed ocean simulations were performed using observed 2000-era sea-surface temperatures (23), with most runs extended for twenty years.

ECHAM5-HAMMOZ is a fully coupled photochemistry-aerosol-climate model, composed of the general circulation model (GCM) ECHAM5, the tropospheric chemistry module MOZ, and the aerosol module HAM. The ECHAM5-HAMMOZ model is described in detail in (24). ECHAM5 is a GCM developed at the Max Planck Institute for Meteorology (25, 26). In this study a T42 resolution was used, corresponding to an Eulerian resolution of ca.  $2.8^\circ \times 2.8^\circ$  degrees, with 31 vertical levels from the surface up to 10 hPa and a time resolution for dynamics and chemistry of 20 minutes. The transport scheme is from (27). The radiative transfer calculation considers vertical profiles of the greenhouse gases (e.g.,  $\text{CO}_2$ ,  $\text{O}_3$ ,  $\text{CH}_4$ ), aerosols, as well as the cloud water and ice.

The chemical scheme has been adopted from the MOZART-2 model (28), and includes 63 transported tracers and 168 reactions to represent the  $\text{NO}_x$ - $\text{HO}_x$ -hydrocarbons chemistry. The sulfur chemistry described by (29) includes oxidation of  $\text{SO}_2$  by OH and DMS oxidation by OH and  $\text{NO}_3$ . The aerosols are described by log-normal modes and are composed of sulfate, organic and black carbon, mineral dust, and sea salt (30, 31). The biogenic monoterpene emissions of (32) are scaled by the factor 0.15 to estimate the production of Secondary Organic Aerosol (SOA) from biogenic sources following (33), SOA is then injected in the atmosphere as primary organic aerosol.

The model has been extensively evaluated in previous studies (24, 30, 34) with comparisons to several measurements and to other model results. In this project the large-scale meteorology is constrained to the year 2000, nudging the temperature, surface pressure, vorticity and divergence to the ECMWF (European Centre for Medium Weather Forecast) ERA40 reanalysis data.

#### *Forcing estimates:*

Emissions scenarios were used in the GISS and ECHAM models, full three-dimensional climate models, to determine the changes in atmospheric composition and the radiative forcing under the scenarios. We make use of the radiative forcing calculated by the two models used here, but those results were scaled according to the best estimates determined from the literature

assessment. Hence the values from the specific models are used as inputs to the analytic temperature projections, but the results are unlikely to be sensitive to potential systematic biases in the models (e.g. the direct forcing from BC being on the low end of the range) due to the scaling to the literature range. The scaling furthermore provides an uncertainty range on the temperature projections that is far more representative of the current state of knowledge than would be results from two models.

Ozone forcing and direct forcings for aerosols were calculated internally within the climate models. The two models produced very similar values for aerosols (within 10%), with somewhat larger differences of 30-50% for ozone in response to the BC measures (Table 1, main text). This suggests that in polluted regions, differences in the background amounts of NO<sub>x</sub> or hydrocarbons in the two models substantially influence the ozone concentration and forcing response to emissions mitigation for CO, NO<sub>x</sub> or hydrocarbons. Forcing from nitrate aerosols is based only on the GISS model as ECHAM did not simulate these aerosols, but this is a very small component of aerosol forcing (global mean .01 W/m<sup>2</sup> or less for the 2030 reference versus 2005 or for any of the 2030 measures versus reference).

The forcing due to methane concentration changes was calculated using the standard IPCC TAR formulation (35), with the concentrations themselves computed internally within the models. Methane concentrations thus respond to changes in oxidants, which control the methane removal rate, as well as changes in emissions of methane itself. Oxidant changes play a role in the methane forcing. Methane has a well known positive feedback on its own lifetime (36), so that the methane emission reductions in the CH<sub>4</sub> measures scenario lead to a shorter lifetime. In the GISS model, the methane residence time decreases from 11.0 years in the 2030 reference case to 9.6 years in the CH<sub>4</sub> measures scenario (versus 10.6 years in 2005). This suggests that the methane feedback on its own lifetime makes a substantial contribution to the -.20 W/m<sup>2</sup> methane forcing in that scenario. The residence time is unchanged adding in the BC Tech measures, but increases back up to 10.2 years in the CH<sub>4</sub> + all BC measures scenario. This indicates that the changes in emissions due to the BC Tech measures have little net global effect on methane oxidation rates, but that changes in emissions that affect oxidation capacity (primarily NO<sub>x</sub> & CO) under the BC Reg measures reduce tropospheric oxidation capacity and cause the resulting increase in methane forcing of .02 W/m<sup>2</sup>. Available ECHAM values are similar, with a methane residence time of 10.4 years in 2005 that increases to 11.1 years in the 2030 reference case, and nearly identical methane forcings in the various scenarios (-.22 W/m<sup>2</sup> for the CH<sub>4</sub> measures, zero for the BC Tech measures, and .02 W/m<sup>2</sup> for the BC Reg measures; Table 1), so that these results appear quite robust.

As aerosol indirect effects (AIE) have very high uncertainties (e.g. (37)) and are difficult to diagnose in climate models, we avoid using results from the pair of models run for this assessment. We instead include an estimate of AIE based on the range of values given in the literature. For scattering aerosols, we use the assumption that they are equal to the direct effect from sulfate aerosols. While there are many studies showing substantial AIE for sulfate aerosols (as many early simulations included only sulfate aerosols), we were unable to find any publications isolating AIE attributable to other scattering aerosol species. In the absence of any quantification of AIE due to OC or nitrate, we assigned the full scattering aerosol AIE to sulfate. Dominance of sulfate in AIE is consistent with its greater solubility and mass relative to carbonaceous or nitrate aerosols, but we caution that apportionment of AIE to individual aerosol species is not well constrained and requires further study. Note that a minimal value of AIE due to OC is consistent with the results from explicit modeling using the GISS-E2 model (see main

text). Calculations based on detailed modeling and observations suggest that the ratio of AIE to direct sulfate RF is 1.5 to 2.0 (38), but we use a lower value of 1.0 as recent analyses based on satellite data suggest that at least a portion of the AIE may in fact be fairly weak (39) and that adjustments to cloud liquid water path may offset changes in particle size (40), and models that now include aerosol effects on mixed-phase clouds tend to show smaller indirect forcings than earlier models (41). Use of the higher 1.5 or 2.0 ratios would have minimal influence on our calculations of the forcing due to the measures investigated here, as these have little effect on sulfate. We include an uncertainty of 66% on the reflective aerosols nitrate and sulfate, for the latter both on the direct and indirect effects (for nitrate assuming their impact is only direct effects), based on a recent assessment (41).

As discussed in depth in the UNEP/WMO Assessment's Chapter 3, there is a wide range of results in the literature for both the direct forcing by BC and for the many indirect effects of BC. Following the discussion there, all the forcing results are scaled to a range of 0.3 to 0.6 W/m<sup>2</sup> as the most probable range for the preindustrial to present-day direct forcing (e.g. (21, 42-44)), with the central value simply the midpoint of this range. Hence the effect of measures are the direct BC forcings calculated in the GISS model, for example, scaled by 0.45/0.32 to get the central estimate of direct forcing from BC and by 0.3/0.32 and 0.6/0.32 to get the lower and upper bounds (the 0.32 is the preindustrial to present-day forcing in the GISS model). Note that the positive scaling for even the central estimate is consistent with the underestimate of AAOD in the model in some regions, as in most models (Table S2). Again based on assessed studies, including (45-48), we assume the combined effect of the semi-direct and indirect effects of BC is from -0.4 to +0.4 W/m<sup>2</sup> from preindustrial to present, and hence add an uncertainty of  $\pm 0.4/0.32$  times the direct forcing calculated in our model. We include BC's effect on snow and ice albedo (49) as an 'effective forcing' 5 times the instantaneous value and hence equal to 0.05 to 0.25 W/m<sup>2</sup> preindustrial to present (50, 51). In this case, rather than base this on the direct forcing, we use the change in BC deposition calculated in the GISS simulations relative to the preindustrial to present-day BC deposition change (the latter was not available for ECHAM, but the deposition changes for other scenarios are quite similar in the two models). Finally, given that there are constraints on the total aerosol forcing, we limit the scalings applied to BC's direct forcing so that the total value cannot exceed 1 W/m<sup>2</sup> based on evidence for a substantial negative net aerosol forcing from a variety of observational and modeling studies (39, 41, 52-56).

For consistency in the treatment of different pollutants, we adopt a similar methodology for organic carbon, scaling GISS results, for example, by -0.20/-0.095 for the central estimate, and -0.09/-0.095 and -0.31/-0.095 for the bounds. For ozone, we scale by 0.35/0.27 for the central estimate, and 0.25/0.27 and 0.45/0.27 for the bounds. These ranges are again based on the evaluations in Chapter 3. This provides a consistent framework for evaluation of the key species involved in our measures other than methane (see below for details on methane). No adjustments were applied to sulfate or nitrate forcings, as these were very similar to the central range from the IPCC AR4 at -0.29 W/m<sup>2</sup> and -0.10 W/m<sup>2</sup>, respectively (GISS model). We assume that aerosol forcings are not independent given constraints on their total, and hence sum these based on their absolute value to obtain upper and lower bounds. The total aerosol forcing and all other forcing uncertainties are assumed to be independent, so the larger values and the smaller values are summed separately to derive upper and lower bounds (we do not sum in quadrature as we do not know the probability distribution within the ranges and we believe that summation in quadrature would produce unrealistically small uncertainties). The process and results of these calibrated forcing estimates are presented in Table S3. Note that the values in the fully interactive GISS

model simulation (Table 1 in main text) are within the uncertainty ranges of the forcings obtained with these estimates. The indirect plus semi-direct forcing of aerosols is substantially larger than the central value of these estimates, however. Furthermore, it is not closely correlated with the direct forcings, indicating that estimates of indirect effects based on proportionality to direct effects must be treated with great caution.

The response to CO<sub>2</sub> emissions was calculated using impulse response functions derived from the Bern Carbon Cycle Model (57) based on the version used in the IPCC TAR. Exponential fits to those functions are used to calculate the CO<sub>2</sub> concentration at a given year resulting from all emissions in prior years. This approach is limited compared with a more sophisticated carbon cycle model, especially in the latter part of the 21<sup>st</sup> century when CO<sub>2</sub> levels become substantially larger in some scenarios and could induce additional feedbacks. Historical emissions of CO<sub>2</sub> are taken from the Carbon Dioxide Information Analysis Center database (58). CO<sub>2</sub> emissions for both the reference and Climate 450 scenarios are from IIASA/GAINS through 2030, and are extrapolated thereafter to 2070 following the IEA 450 scenario (from 2030-2050, for example, CO<sub>2</sub> emissions increase by ~12 Gt per year in the reference scenario but decrease by ~16 Gt per year under the 450 scenario). We also perform an offline calculation of the methane response to changes in methane emissions over time using an analogous model but with a single impulse-response function that uses the methane lifetime. Emissions under the reference or Climate 450 scenarios were used along with the lifetime calculated for those scenarios in the full global composition model (emissions after 2030 are assumed to be constant). For other scenarios, the difference between the average year 15-19 methane abundance simulated in the full composition model and the baseline model was linearly imposed upon the baseline concentration trends between 2005 and 2040 (as the bulk of the response to emissions changes through 2030 would have been realized given a decade or more response time). Radiative forcing from CO<sub>2</sub> and methane are calculated using the standard IPCC TAR formulation (35), with an uncertainty of 10% for the radiative effect of each as in previous studies (e.g. (43) plus additional uncertainties of 1% for the methane response to OH changes (36) and 5% for CO<sub>2</sub> to account for carbon-cycle feedbacks. All values are instantaneous forcings at the tropopause.

Finally, to facilitate comparison with studies that have presented preindustrial to present-day changes, we report some aspects of the BC simulations of changes over this time in the GISS simulations. Emissions changes were 5.00 Tg BC yr<sup>-1</sup>, which lead to an increased load of .17 mg m<sup>-2</sup>. The lifetime of this increased BC was 6.4 d, and the resulting global mean BC AAOD was .00113, implying a mass absorption coefficient of 6.6 m<sup>2</sup> g<sup>-1</sup>. This led to the BC direct radiative forcing of 0.32 W m<sup>-2</sup> given above, which was then scaled to 0.45 W m<sup>-2</sup> for the industrial period (implying a similarly adjusted load or AAOD).

#### *Analytic temperature change estimates:*

We estimate the surface temperature response to the calculated radiative forcings following the methodology used in calculation of global temperature potentials (59). This is further extended to regional temperatures following the method described in (60). In essence, we obtain a rough approximation of global and regional responses by multiplying the calculated RF by the global or regional transient sensitivity and, accounting for ocean inertia by including a tapering influence of forcing during the prior 20 years (based on a fit to the prior model runs). While many simple global energy balance models exist, our calculations allow estimation of regional

responses including the influence of both local and remote forcings using the results of (55) and the spatial patterns of forcing calculated here.

In our calculations, the surface temperature change in area  $a$  between time 0 and time  $t$  is given by:

$$dT_a(t) = \int_0^t ((k_{SHext,a} * F_{SHext}(t') + k_{Tropics,a} * F_{Tropics}(t') + k_{NHml,a} * F_{NHml}(t') + k_{Arctic,a} * F_{Arctic}(t')) / k_{Global,a} * f(t-t') dt'$$

where  $F_{area}$  is the radiative forcing in the particular area (NHml is Northern Hemisphere mid-latitudes, SHext is Southern Hemisphere extratropics), and the  $k_{x,a}$ 's are the response coefficients giving temperature response in area  $a$  to forcing in area  $x$  (55) (Table S4). The first term in the integral represents the RF weighted by regional sensitivities while the second term,  $f(t)$ , describes the climate system's inertial response. The latter is defined as:

$$f(t) = 0.541/8.4 \exp(-t/8.4) + 0.368/409.5 \exp(-t/409.5)$$

where  $t$  is the time in years and the two exponentials represent the relatively rapid response of the land and upper ocean and the slower response of the deep ocean based on exponential fits to the response in simulations with the Hadley Centre climate model (61, 62), with absolute responses scaled by 0.857 to match the transient climate sensitivity of the GISS model (0.53 C per W/m<sup>2</sup> for increasing greenhouse gases) for consistency with the other model results used here (and as the sensitivity in the simulations used to derive the responses was high even compared with standard Hadley Centre simulations).

We note that the climate system's response to different forcing agents is not identical. In particular, some forcing agents such as BC have a substantially different efficacy than CO<sub>2</sub> (43, 63). Such variations in efficacy arise partially because of the inhomogeneous distribution of forcings (55), which is accounted for in our use of regional temperature potentials. In the case of BC, much of the divergence appears to be related to its strong semi-direct effect, which is not included in traditional definitions of radiative forcing used in calculating efficacies. As the semi-direct effect is explicitly included in our analysis, the efficacies for the various forcing agents are likely to be fairly uniform, though they would in fact contribute slightly to uncertainty in the climate response. Although such uncertainty is not included here, the prior studies of efficacy, suggest that any residual non-uniformity would be minor, given that we account for two of the largest sources of non-uniformity, and certainly small in comparison with the uncertainty in the overall climate sensitivity (+50%/-33%), which is included in our calculations. Feedbacks of climate change on atmospheric composition, and hence radiative forcing, are also not included in our analysis. However, these have generally been small in prior studies in comparison with the effects of emissions changes (e.g. (64)).

Historical forcing is based solely on CO<sub>2</sub> emissions as forcing from CO<sub>2</sub> alone is approximately equal to the net forcing to date (43), so that the inertial response to historical CO<sub>2</sub> forcing provides a good estimate for the total inertial climate response. Forcings for aerosols and ozone were linearly interpolated between 2010 and 2030. We assumed that these forcings remained constant after 2030 in these temperature response calculations. Methane emissions also remained constant after 2030, though methane concentration continued to evolve. Carbon dioxide emissions were linearly extrapolated past 2030, increasing at 1.53% per year in the reference scenario and decreasing by 0.84% per year under the low-carbon scenario. Calculations

were performed for each latitude band and for the global mean. Uncertainties were derived by adding the forcing uncertainty in quadrature with the uncertainty in climate sensitivity, where for the latter we use the 2 to 4.5 C range about a central estimate of 3 C for a doubling of CO<sub>2</sub> given in (65) and deemed there to represent the 67% confidence interval for climate sensitivity (corresponding to a transient climate response of 1.3 to 3 C for a doubling of CO<sub>2</sub>). In cases with large forcing from BC, uncertainties may be even larger as the surface temperature response per unit radiative forcing can vary substantially depending on the vertical profile of the BC (63).

Regional estimates of temperature change from climate models are not reliable in many cases. Hence we base our estimates of the regional temperature response to the measures analyzed here on the regional temperature changes calculated for each latitude band. We first multiplied the temperature changes by the ratio of land area versus the total latitude band change seen in observations (66) to account for the more rapid response of land to forcing. For each region, we then averaged the temperature changes by latitude band weighting the result by the land area of that region within each band.

The uncertainty in the temperature responses comes from the underlying radiative forcing, the difference between the ECHAM and GISS models, and the climate sensitivity. Note that we do not include any uncertainties in the emissions changes brought about by the measures, though these may be substantial as base emission inventories themselves vary greatly (67).

An example of the application of the analytic temperature change calculations is the effect of a delay in implementation of the measures. Phasing in the measures 20 years later than examined in the full climate simulations or the primary analytic estimates results in a commensurate delay in the climate mitigation, but has very little effect on long-term climate (Figure S3). This highlights how the timing of emissions reductions of short-lived climate forcers is important for near-term climate, but that provided such controls are eventually put into place has little effect on long-term climate. Such a result emphasizes the distinct nature of near-term and long-term climate change and the distinct mitigation actions needed to affect the two timescales.

### *Climate Simulations:*

Climate simulations were performed with the GISS-E2-S model, the full atmospheric GISS-E2 model (including chemistry and aerosols) coupled to a mixed-layer or ‘slab’ ocean. These include equilibrium calculations for the 2030 reference case and for the 2030 methane + all BC measures case. These simulations were run for 50 years, with analyses of the last 20. Two additional calculations were performed with the same emissions but using fixed sea-surface temperatures and sea ice coverage to diagnose the forcing from cloud and albedo changes. The only difference between these latter two runs was thus the emissions of aerosol (and ozone) precursors, and hence the changes in BC deposition and cloud cover can be attributed to the aerosols (rather than to factors such as climate feedbacks). These runs were also performed for 50 years. The results of those simulations are compared with results from the same model in a simulation driven solely by changing greenhouse gas (CO<sub>2</sub>) concentrations. This serves as an analogue for the response to the methane measures, which cause globally quasi-uniform forcing by altering greenhouse gases (methane and ozone, with the latter having worldwide changes since it is responding to global methane changes). The response to doubled CO<sub>2</sub> changes is normalized by the ratio of the forcing ( $-0.32 \text{ W/m}^2$ ) seen in the GISS methane measures

simulations with doubled CO<sub>2</sub> forcing. It would be useful to verify the assumed linearity of the response to greenhouse gas forcing.

Regional results in the mixed-layer climate model runs showed the Northern Hemisphere extratropics warming by  $0.70 \pm 0.12^\circ\text{C}$  ( $0.61 \pm 0.14^\circ\text{C}$  from 30°N-60°N and  $0.93 \pm 0.26^\circ\text{C}$  from 60°N-90°N) in response to the CH<sub>4</sub> and BC measures, in good agreement with the warming of  $0.73 \pm 0.4^\circ\text{C}$  using the analytic equations and forcings from the composition models calibrated to the literature ( $0.73 \pm 0.29/0.51^\circ\text{C}$  from 30°N-60°N and  $0.72 \pm 0.49/0.57^\circ\text{C}$  from 60°N-90°N). The climate model shows more warming at high Southern latitudes, however, where results from the mixed-layer ocean model likely overestimate responses by not allowing oceanic current changes that would tend to reduce local maxima in warming in the Southern Ocean (Figure 2, main text). Comparison of the  $-0.54^\circ\text{C}$  global mean equilibrium response in the coupled model with  $-0.77 \text{ W/m}^2$  global mean forcing (Table 1, main text) gives a climate sensitivity of  $0.70^\circ\text{C}$  per  $\text{W/m}^2$ , a value in good agreement with the range inferred from paleoclimate data, recent climate change, and modeling (65). National scale results from the climate model simulations were shown in Figure 4, and numerical values for the countries with largest impacts are presented in Table S5 (along with the other impacts shown in Figure 4).

As noted in the main text, the two models used to evaluate forcing have reasonably good representations of present-day atmospheric forcing in comparison with a semi-empirical estimate (56) (Figure S4). An alternative geographical presentation of the atmospheric forcing data is given in Figure S5 (along with other impacts shown in Figure 4).

#### *Agricultural Impacts:*

Ozone-related crop yield changes were calculated for wheat, rice, maize and soybeans following (68). The ozone exposure indicator used was the seasonal mean daytime ozone concentration, indicated as M7 for the 7 h mean (09:00–15:59) or M12 for the 12 h mean (08:00–19:59), depending on which had been reported for the particular crop. These metrics were calculated for the crop-specific growing season (with a standard duration of 3 months) depending on location. The methodology for the definition of the growing season makes use of multiple data sources, including temperature data, reports describing the growing season for major crops, and location of different climate zones, as described in (68).

We note that the concentration-response relationships are ‘pooled’ based on a variety of cultivars that are grown in the US and Europe. They are considered to reliably represent the average response of the commonly grown cultivar population on national or regional level in those regions. Small-scale individual studies indicate that Asian cultivars for winter wheat and rice are equally or more sensitive to ozone damage than the US cultivars (69), hence our results applying the US-derived exposure–response relationship are likely to be on the conservative side.

As described in more detail in (68), the spatial distribution of crops and their production numbers are calculated on a  $1^\circ \times 1^\circ$  grid resolution, based on crop suitability indices for each of the crops considered. Crop suitability grid maps are taken from (70). In particular, national production numbers (obtained from the FAO) are distributed over ‘suitable’ crop production grid cells with a weight defined by the appropriate crop suitability index. The ozone metrics are calculated for each grid cell, hence crop production loss is obtained at grid cell resolution, and afterwards aggregated to national totals. All base crop production levels are present-day rather than projections for 2030.

The uncertainty range in the crop yield losses comes from both concentration-response function uncertainties and differences between the ECHAM and GISS modeled ozone. For the methane measures, these two factors have comparable uncertainties, while for the BC measures the model-to-model differences in ozone responses are dominant. We also note that the effects of increasing CO<sub>2</sub> on ozone-related crop damage (71) have not been included here, but these may lessen the impact of future ozone-related crop yield losses and merit further analyses.

### *Health Impacts:*

Surface composition simulated in the two GCMs was used as the basic input to the health calculation. We used annual mean modeled surface PM<sub>2.5</sub> exposure (excluding dust and sea-salt) and the 6-month maximum of the averaged 1-hr daily maximum ozone concentrations. Modeled PM<sub>2.5</sub> distributions were downscaled to 0.5 x 0.5 degrees using a subgrid parameterization of urban/rural differences, while for ozone, we calculated health impacts using ozone at the GCMs' native resolutions, but using population data at 0.5 x 0.5 degrees. We did not apply a sub-grid correction for urban titration effects (urban ozone decrement). As BC and OC have short lifetimes and their concentrations are driven by primary emissions, their abundances are expected to be closely related to population density. Therefore the downscaling for PM<sub>2.5</sub> brought these components of the PM<sub>2.5</sub> distributions to 0.5 x 0.5 degrees using a subgrid parameterization of urban/rural differences developed at the Joint Research Center. The parameterization is based on a population-based re-distribution of the primary PM<sub>2.5</sub> concentration (BC and OC) on a 0.1°x0.1° degree sub-grid, within each GCM surface grid cell. Population data at the subgrid resolution are from the Gridded Population of the World Version 3 (Center for International Earth Science Information Network, Columbia University, <http://sedac.ciesin.columbia.edu/gpw>, 2005). These were used to determine the urban area fraction  $f_{ua}$  and urban population fraction  $f_{up}$  within each native grid cell, using a threshold population density of 600 persons per square km. We then made the simple assumption that the primary rural BC concentration rescales to  $(1 - f_{up})/(1 - f_{ua}) \times BC_{GCM}$  and the urban concentration to  $f_{up}/f_{ua} \times BC_{GCM}$ , which preserves the larger GCM grid box average. This assumption implies that the urban and rural emissions are mixing and diluting at the same rate. In the calculations performed here, we impose a minimum value on the rural BC concentration of one-half the GCM concentration, and then set a maximum on the urban concentration of 5 times the rural value. The 0.1 x 0.1 degree population and exposure-weighted results are then aggregated to a 0.5 x 0.5 degree grid for the health analyses. This same downscaling has been used previously, and shown to increase the agreement between the modeled PM<sub>2.5</sub> and urban observations in China and North America (72). We include PM mortalities due to cardiopulmonary illness and lung cancer calculated using relative risk estimates from (73) and ozone mortalities calculated using relative risk estimates for respiratory disease from a two-pollutant model (74). The uncertainty range in the health calculations comes from both concentration-response function uncertainties and differences between the ECHAM and GISS modeled PM<sub>2.5</sub> and ozone. Separation of these two components indicates that the uncertainty in the concentration-response relationship is dominant, with uncertainty in atmospheric processes, as represented by GISS/ECHAM model differences, playing a minor role. All are based on 2030 population estimates.

The health impact calculations follow established epidemiological concentration-response functions and are described in detail by Anenberg et al. (in prep.). For PM<sub>2.5</sub>, we use cardiopulmonary and lung cancer relative risk estimates from the American Cancer Society

(ACS) Study (75). For a 10  $\mu\text{g}/\text{m}^3$  increase in annual average  $\text{PM}_{2.5}$ , relative risks of death due to cardiopulmonary disease and lung cancer are 1.09 (95% confidence interval [CI]: 1.03-1.16) and 1.14 (95% CI: 1.04-1.23). We multiply these estimates by 1.8, consistent with the mean all-cause relative risk estimate from a US Environmental Protection Agency expert elicitation which suggests that the ACS study underestimated  $\text{PM}_{2.5}$  mortality risk (76). For ozone, we use long-term relative risk estimates from the two-pollutant model calculated by (74), also based on the ACS cohort. For a 10 ppb increase in seasonal (6 month) average 1-hr daily max ozone, relative risk of respiratory mortality is 1.04 (95% CI: 1.013-1.067). Consistent with the ACS cohort, we include only the population over 30 years of age, and for the 2030 calculations include projected changes in population (amount and distribution) following a conservative B2 scenario (77) (global population increases from 6.5 billion in 2006 to 8.4 billion in 2030). The calculations also include worldwide variations in underlying baseline mortality, as described in (78). While mortality rates are expected to change over the next several decades, projected mortality rates for future years are not available, hence current incidence rates were used to estimate 2030 incidence.

Uncertainties in mortality calculations include the 95% CI in the concentration-response function derived from epidemiological studies and the variation between the two models. Assessing the global health impacts of air pollution is subject to a variety of other uncertainties that are not easily quantifiable. We do not explore uncertainties in emissions changes due to application of emissions control technologies, for example. In the absence of long-term air pollution mortality studies in the developing world, we also assume the concentration-response relationships found by Jerrett et al. (2009) and Krewski et al. (2009) in the US apply to the rest of the world, despite substantial differences in exposure levels,  $\text{PM}_{2.5}$  composition, and lifestyle. In particular, while the  $\text{PM}_{2.5}$  data used to develop the concentration-response relationships in Krewski et al. (2009) ranged up to 30  $\mu\text{g}/\text{m}^3$ , predicted  $\text{PM}_{2.5}$  concentrations in the 2030 baseline scenario ranged as high as 73  $\mu\text{g}/\text{m}^3$  (excluding dust and sea-salt). Some evidence from indoor air pollution exposure and cigarette smoking suggests that the concentration-response relationship may flatten at high concentrations (79, 80). However, since this relationship is not yet well characterized at high concentrations, we extrapolate relative risk estimates linearly from low concentrations to high concentrations. If the relationship flattens at high concentrations, these results would be overestimates. However, since the model may sometimes underestimate concentrations in urban areas in the developing world (72), these biases may offset one another to some extent. We also assume that all  $\text{PM}_{2.5}$  components and mixtures are equally toxic, despite wide variation in air pollution mixtures around the world. Though there is some evidence that some mixtures are more toxic than others (e.g. (81, 82)), we do not believe that the current available data is adequate to separate health impacts by component. While populations around the world vary in age structure, medical care, and exposure patterns, extrapolation of relative risk estimates found in the US is supported by general consistency among short-term epidemiology studies around the world for both ozone and  $\text{PM}_{2.5}$  (83, 84). Since causes of death differ dramatically around the world, we calculate cause-specific mortality, which may be more comparable around the world than all-cause mortality.

Benefits to public health from improved indoor air quality have been estimated for India and China only, due to data limitations (see main text). Reducing emissions of BC and CO from biomass combustion will result in reductions in exposure to those combustion products indoors, with attendant health benefits. We have taken data from the Global Burden of Disease report of 2004 for the burden of solid fuel use in the domestic sector in those countries in 2000 (85). This

report provides a summary of the health effects and the dose-response relation. Work by IIASA for the new Global Burden of Disease report contains estimates of exposure for 2030 under the reference scenario, and under the alternative scenario. From these, we can estimate the difference in health burden. These are again presented as deaths per year avoided by the strategy, and years of life lost. Again, we have held mortality rates constant in our analysis, which may be conservative. Using this methodology, we estimate 220,000 deaths could be avoided each year in India due to reduced indoor air pollution if all BC measures were implemented. In China, we would see a reduction of 153,000 deaths per year.

### *Economic Valuations:*

Valuation of climate benefits of methane emissions reductions is based on converting those into CO<sub>2</sub>-equivalent using GWP100 and then multiplying by the SCC. Values in Table 2 include uncertainties based on the fractional uncertainty in the climate response. The influence of alternative SCC values or metrics is discussed in the text. All values are 2006 \$US. Valuation of the climate benefit for the BC measures are based on the climate benefits for the methane measures times the relative climate impact of the BC measures in order to account for the various factors affecting climate that do not have values of metrics such as GWP (e.g. aerosol indirect effects).

As noted in the main text, a GWP-based valuation neglects differences in the regional effects of these pollutants on temperatures, precipitation and sunlight available for photosynthesis relative to CO<sub>2</sub>. As Figure 2 in the main text shows, regional effects can be quite distinct in the case of the BC measures. Additionally, the SCC includes some CO<sub>2</sub>-specific factors such as fertilization of ecosystems which would not be present with forcing from methane or other short-lived species. As damages are often thought to scale as a power of temperature change, there may also be somewhat less valuation of near-term changes than of later changes in a warmer future world and the climate valuation would grow more sharply with time for short-lived species than for CO<sub>2</sub>. Further work is clearly needed to better define appropriate techniques for valuation of non-CO<sub>2</sub> climate impacts.

Valuation of premature mortalities is based on the value of a statistical life (VSL) approach (86, 87). The relationship between mortality risks and willingness-to-pay (WTP) is used to determine the VSL, which is an expression of the value that people affix to small changes in mortality risks in monetary terms. We employ the United States Environmental Protection Agency's (USEPA) preferred VSL of \$9,500,000 for 2030. This value represents the mean of 26 peer-reviewed studies (88), inflated to 2030 based on projected income growth.

Our first approach applies the USEPA value uniformly across all countries, so that mortality risks are valued equally worldwide. While ethically appealing, the VSL is based on society's WTP for mortality risk reduction and WTP is a function of income. Hence, it is likely that WTP will vary by country. This motivates the second approach in which the USEPA VSL is adjusted. We employ the USEPA's elasticity of 0.40 between income and WTP to estimate country-specific VSLs based on the relationship between country-specific income per capita and that in the U.S (88) using income data reported by the World Bank (89). In order to compute the VSL in a particular country that lacks a credible VSL estimate (VSL<sup>1</sup>), the VSL in a country in which there is a reported VSL estimate (VSL<sup>2</sup>), is multiplied by the ratio of per capita incomes (Income<sup>1</sup>/Income<sup>2</sup>) raised to the power of the selected income elasticity (0.40, in this case): VSL<sup>1</sup> = VSL<sup>2</sup> \* (Income<sup>1</sup>/Income<sup>2</sup>)<sup>0.40</sup>. The income elasticity applied in this analysis (0.40) reflects that

used by USEPA in analyses that require adjustments of estimated VSLs to projected changes in personal income. Although USEPA applies this value only to future growth in the aggregate GDP, we apply it here to adjust VSL from the US to other countries. This approach was applied to estimate a country-specific VSL for each of the approximately 210 countries encompassed in the analysis. Note that the approach assuming that the VSL is equal across all countries in effect sets the elasticity to zero. Valuations in the main text are presented using country-specific VSLs. Valuation using uniform VSL is presented in the UNEP/WMO Assessment (1).

Valuation of crop yield changes uses year 2000 global market prices from the Food and Agriculture Organization (faostat.fao.org), which clearly does not account for benefits such as those to subsistence farmers or to national food security. Valuation for other effects of air quality, such as changes in forestry yields, tourism or depreciation of man-made materials, is not included.

Mitigation cost estimates in the main text are given from analyses by the IEA and with the GAINS model. The latter has been used recently for evaluation of the European Union effort-sharing decision (90, 91).

#### *Regional and National level results for individual crops:*

The analysis shown in the main text summed the change in wheat, rice, maize and soybeans. Impacts of the measures were also analyzed for individual crops (Figure S6).

For wheat, the greatest benefits are in India and China, followed by Pakistan, but there are also large benefits in northern countries including the US, France, Russia, Italy, Germany and the UK. Large gains in tonnage of wheat yield are also seen in the Middle East, especially in Turkey and Iran. Looking instead at the percentage change in wheat yield, improvements are greatest in countries of the Middle East and South Asia. A variety of other countries show large percentage improvements, including nations in Southern Europe, China, Japan, and Mexico. The northern European countries and the US, noted above as having large gains in tonnage of wheat, do not stand out in percentage, however.

Turning to rice, the total tonnage gains are heavily dominated by improvements in India and China. In percentage terms, however, countries in the Middle East and both Central and South Asia show the greatest gains. Several countries in East Asia, including China, Japan and the Koreas also show large improvements. For rice, large benefits are also seen in several Western Hemisphere countries, including the US and several central American nations.

Examining changes in tonnage of maize, China shows the largest gains, but India is much further down the list. Instead, the United States is second, Mexico third, and several countries in South Asia, the Middle East, Europe and Brazil make up the next group. In percentage terms, again the yield gains are greatest in South Asian and Middle Eastern countries. For soybeans, the rankings are quite different in terms of tonnage, with the largest increases in the USA, China, Brazil, Argentina, and India (in that order). In percentage, however, the gains are again greatest in South Asia and the Middle East.

Although all the crop yield changes are based on the same modeled ozone response to the measures, the relative impact in different countries varies from crop to crop. This is true even for wheat and rice, which use the same ozone metric in the concentration-response relationship (M7). For example, the gain in yield in Pakistan compared to the US is 2.7x larger for wheat, but only 1.4x larger for rice. Similarly, the yield gain in Iran is 1.5x larger in Iran than in Pakistan for

wheat, but 3.1x larger for rice. This highlights how the yield gains are sensitive to the ozone concentration change in the part of the country where each particular crop is grown.

We can also separate the effects of the methane measures, which affect background ozone worldwide, from the more localized BC measures. The methane measures are responsible for approximately half (49-57%) of the wheat yield improvements in China, India, Nepal and Pakistan. In these countries, yield improvements in other crops tend to result more from the BC measures, with anywhere from 25% to 58% of the gains attributable to the methane measures (32-39% in China). Similarly, the methane measures contribute a bit less than half (41-45%) the large gains in soybean yields in Brazil and Argentina and in maize in Mexico. In the US, distant from where the emissions reductions take place, the methane measures account for the bulk (60-76%) of the crop yield benefits (values are similar for Europe, e.g. 65-76% of benefits in France, Italy, Germany and the UK).

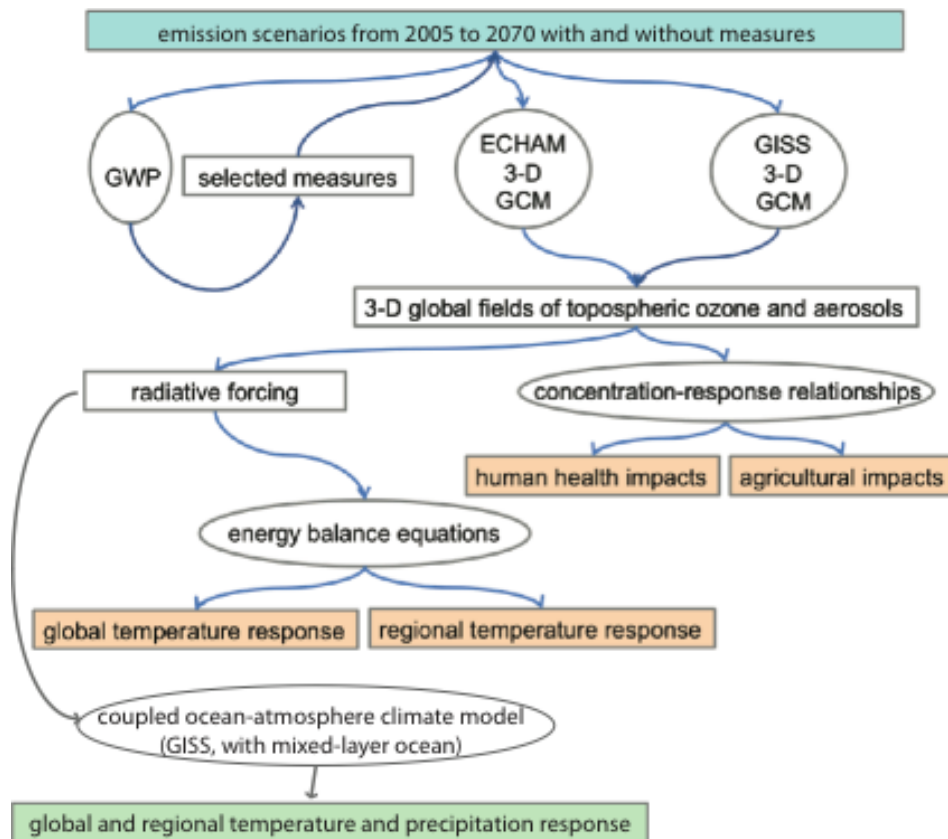


Figure S1. The chain of calculations used in the identification of measures and analysis of their impacts. BC and methane emission control measures are imposed over 2010 to 2030.

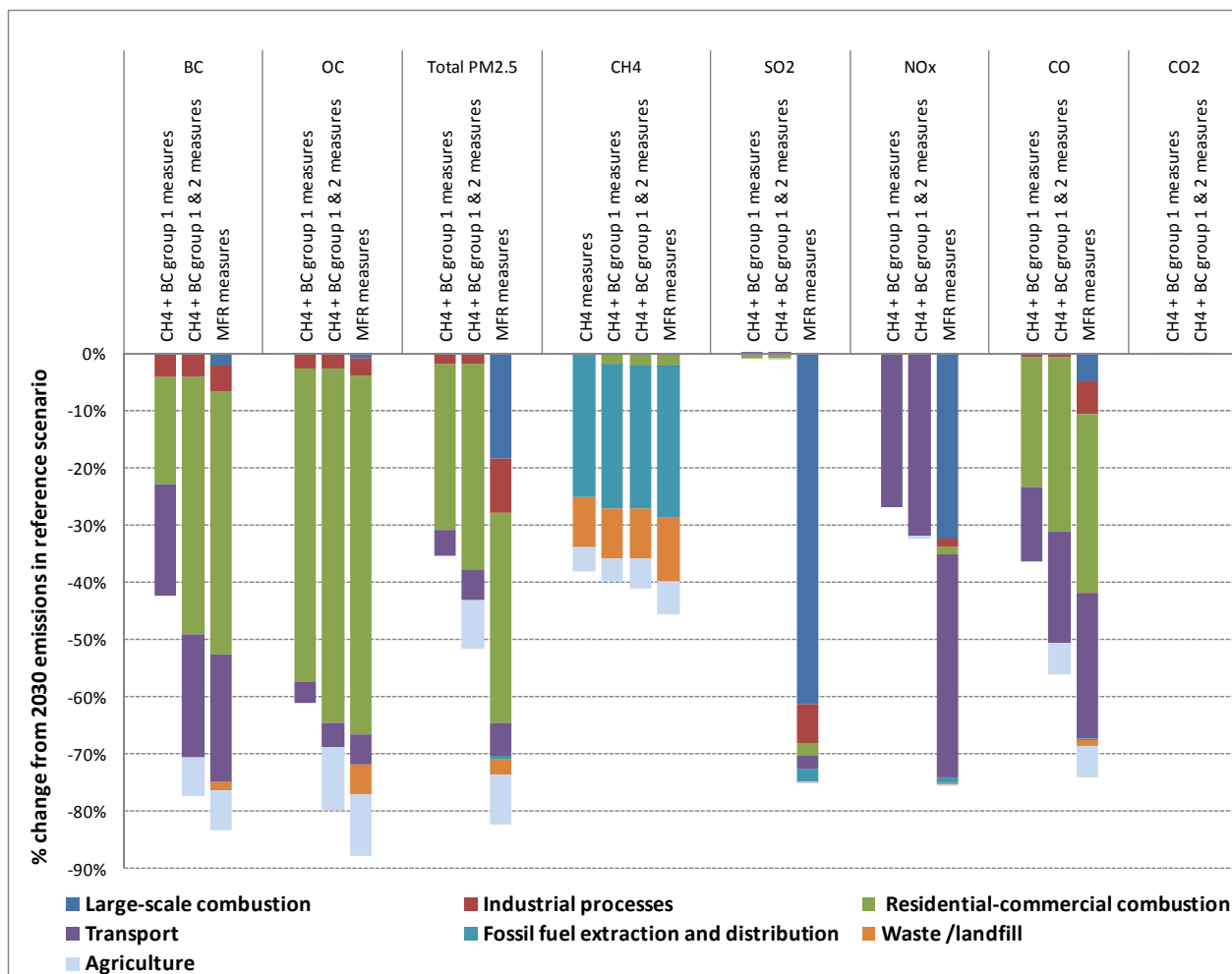


Figure S2. Emission reductions in 2030 from the three sets of measures compared to the reference scenarios. Group 1 are the BC ‘Tech’ measures, Group 2 are the BC ‘Reg’ measures, and MFR are the emission reductions from application of all ~400 measures. The methane emissions changes for the methane measures are 139 Tg yr<sup>-1</sup>. For the ‘Tech’ and ‘Reg’ measures, respectively, changes by emitted species are: BC 2.21 and 4.04 Tg C yr<sup>-1</sup>, OC 7.91 and 10.4 Tg C yr<sup>-1</sup>, CH<sub>4</sub> 145 and 150 Tg yr<sup>-1</sup>, SO<sub>2</sub> 0.89 and 0.89 Tg SO<sub>2</sub> yr<sup>-1</sup>, NO<sub>x</sub> 7.37 and 8.92 Tg N yr<sup>-1</sup>, CO 197 and 305 Tg yr<sup>-1</sup>, and CO<sub>2</sub> 19 and 19 Tg CO<sub>2</sub> yr<sup>-1</sup>.

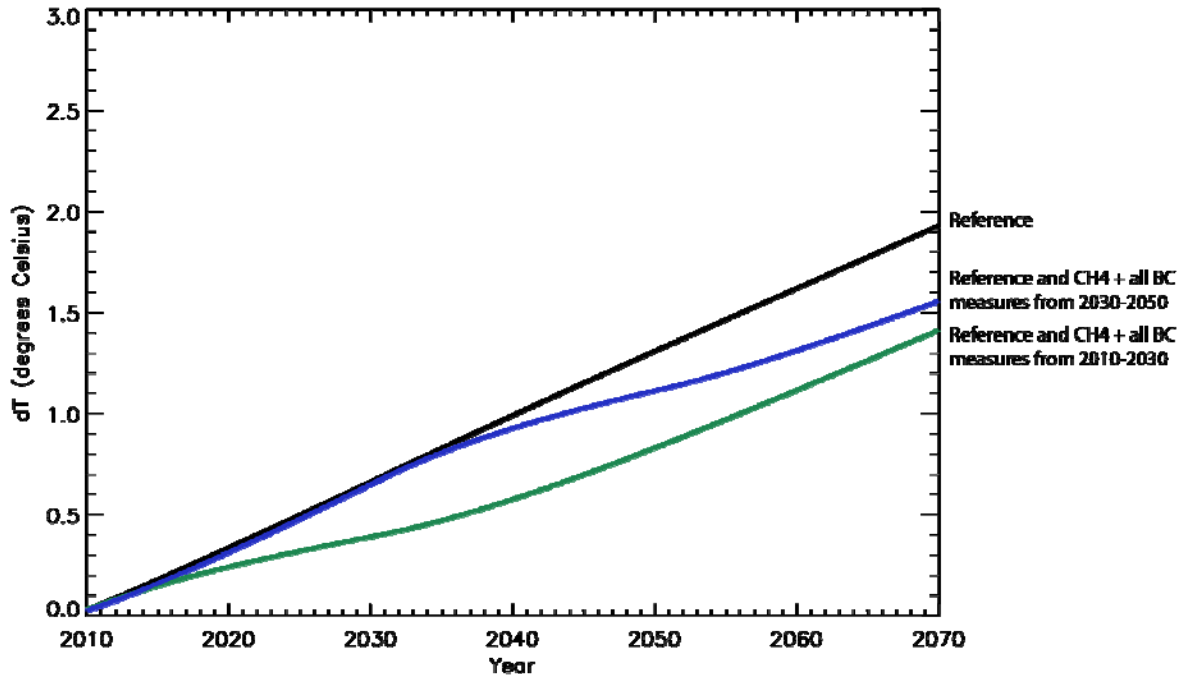


Figure S3. Projected global mean temperature changes for the reference scenario and for the reference plus measures to limit methane and BC emissions immediately or delayed by 20 years. Values calculated using the analytic temperature change estimate methodology.

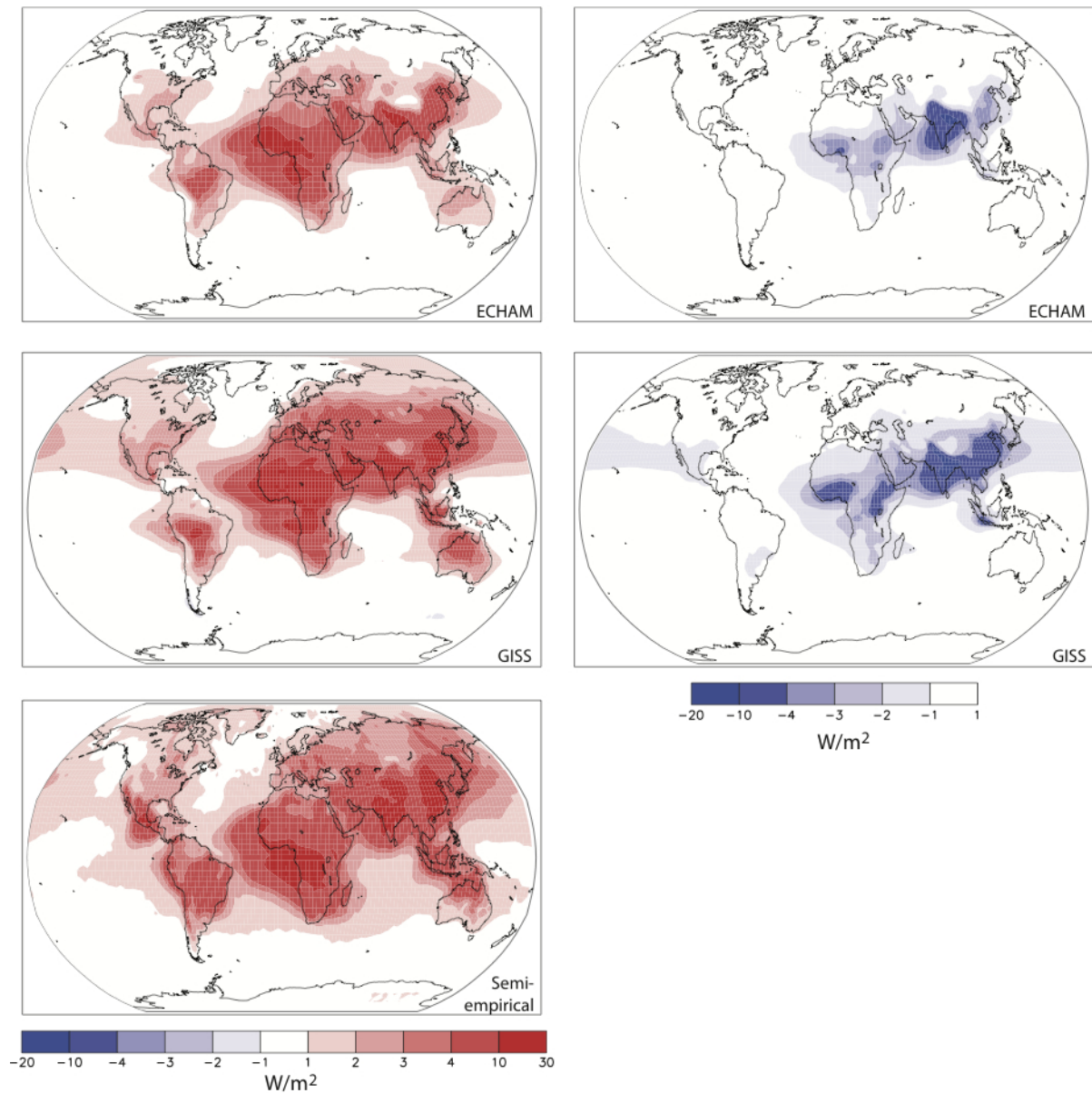


Figure S4. Total present-day atmospheric forcing (TOA minus surface;  $\text{W/m}^2$ ) in the ECHAM model (top left), the GISS model (center left), and the semi-empirical estimate of (42) (lower left), and the changes resulting from the implementation of all measures (right column).

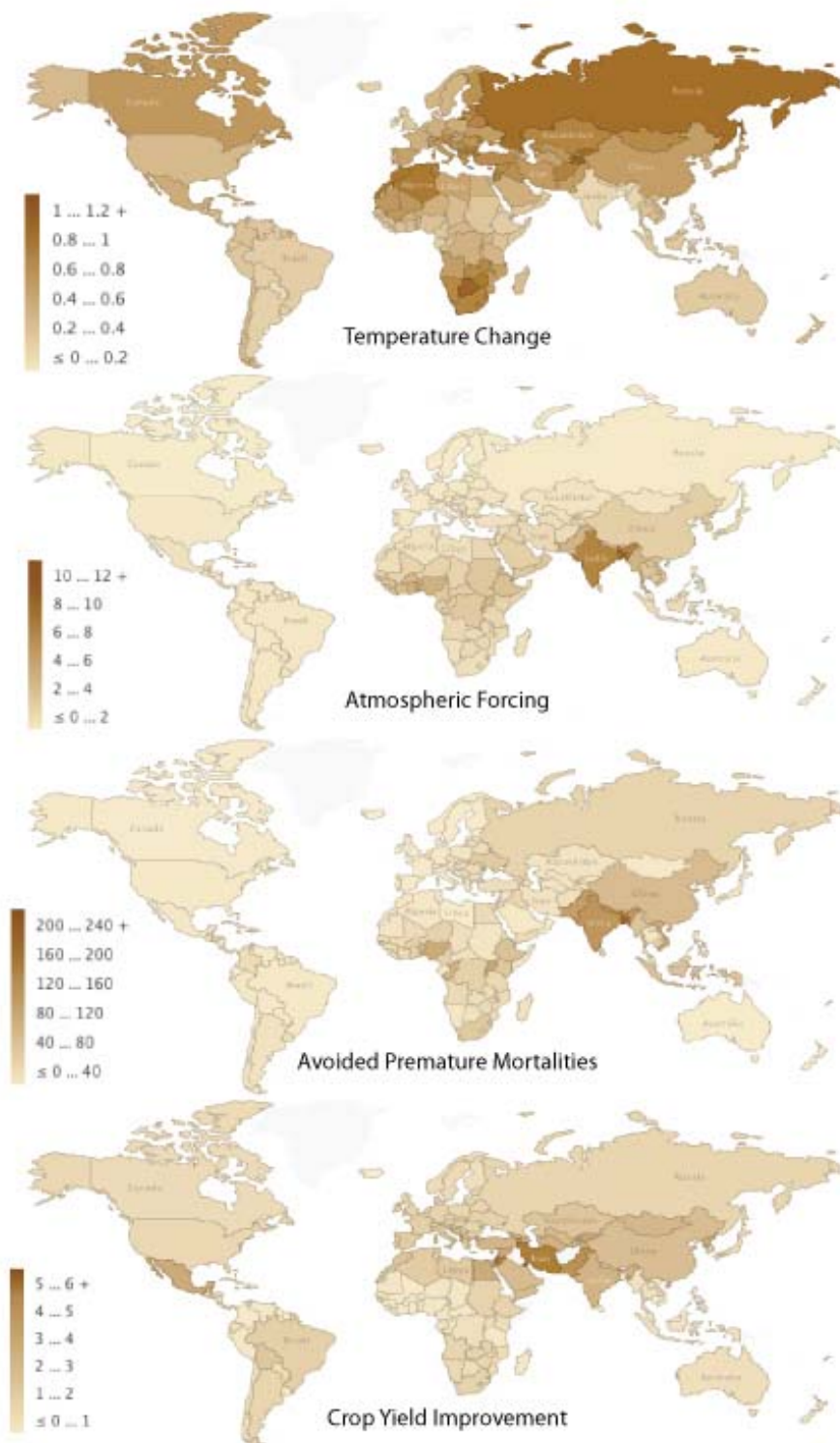
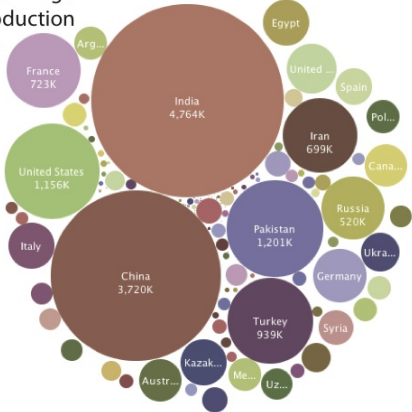


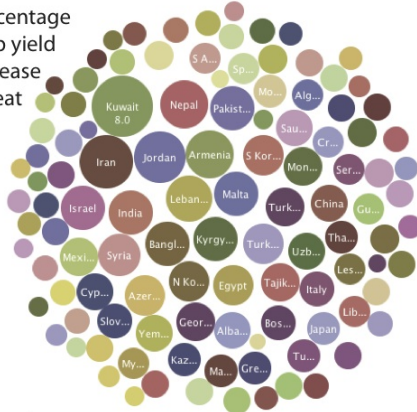
Figure S5. Benefits of CH<sub>4</sub> and BC measures in reduced temperature change (top; °C), reduced atmospheric forcing (2<sup>nd</sup> row; W/m<sup>2</sup>), for human health (3<sup>rd</sup> row; annually avoided premature deaths per 100,000 persons over age 30), and agriculture (bottom; annual percentage crop yield

increase, sum of wheat, rice, maize and soy) as in Figure 4. Interactive versions providing values for each country are at <http://www.giss.nasa.gov/staff/dshindell/Sci2012/>.

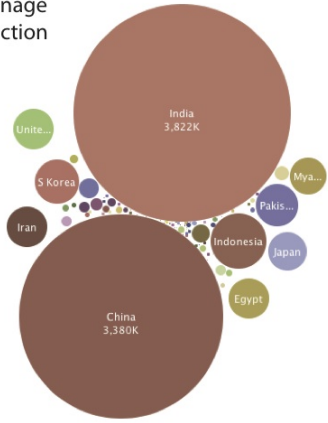
Annual tonnage  
crop production  
increase  
wheat



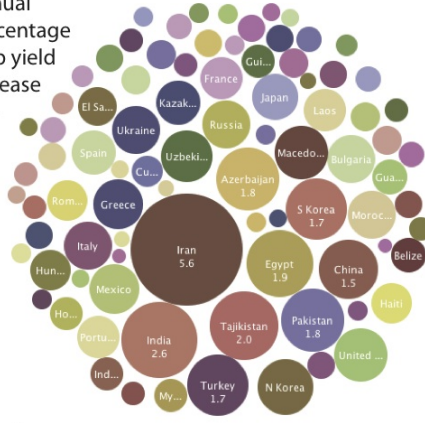
Annual  
percentage  
crop yield  
increase  
wheat



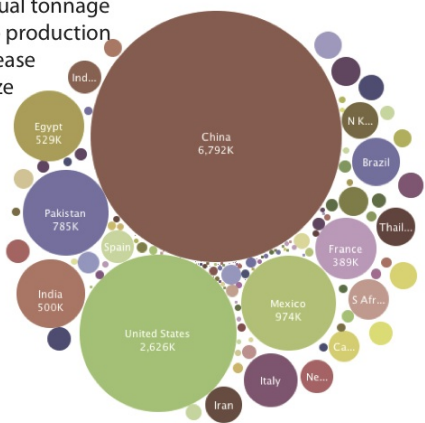
Annual tonnage  
crop production  
increase  
rice



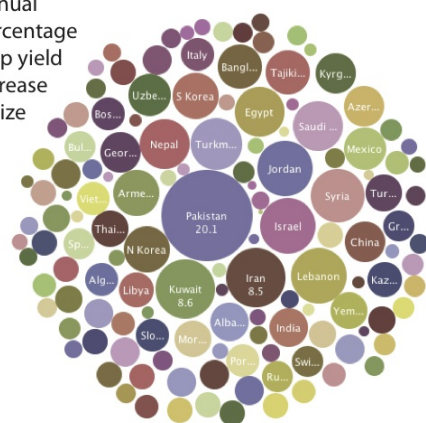
Annual  
percentage  
crop yield  
increase  
rice



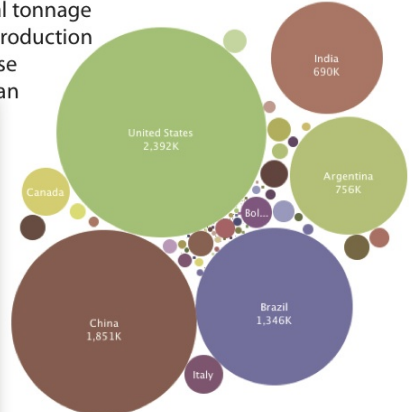
Annual tonnage  
crop production  
increase  
maize



Annual  
percentage  
crop yield  
increase  
maize



Annual tonnage  
crop production  
increase  
soybean



Annual  
percentage  
crop yield  
increase  
soybean

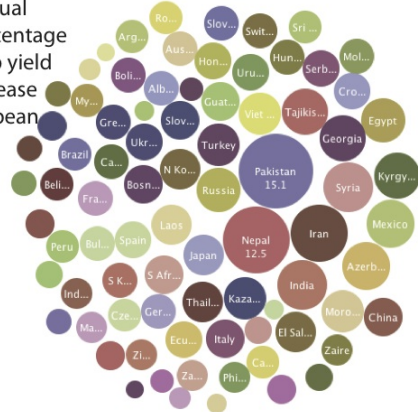


Figure S6. Country and crop specific yield impacts for 2030 for all measures versus the reference scenario. Values are shown for avoided crop yield losses (in tons on left, in percent on right) for wheat (1<sup>st</sup> row), rice (2<sup>nd</sup> row), maize (3<sup>rd</sup> row) and soy (4<sup>th</sup> row). Impacts are based on the GISS/ECHAM average concentration response, with uncertainties as in the main text. Interactive versions providing values for each country are available at <http://www.giss.nasa.gov/staff/dshindell/Sci2012/>

Table S1. Methane and BC measures identified as mitigating climate change and improving air quality which have a large emission reduction potential<sup>1</sup>.

Measure	Sector
<b>CH<sub>4</sub> measures</b>	
Extended pre-mine degasification and recovery and oxidation of CH <sub>4</sub> from ventilation air from coal mines	Extraction and transport of fossil fuels
Extended recovery and utilization, rather than venting, of associated gas and improved control of unintended fugitive emissions from the production of oil and natural gas	
Reduced gas leakage from long-distance transmission pipelines	
Separation and treatment of biodegradable municipal waste through recycling, composting and anaerobic digestion as well as landfill gas collection with combustion/utilization	Waste management
Upgrading primary wastewater treatment to secondary/tertiary treatment with gas recovery and overflow control	
Control of CH <sub>4</sub> emissions from livestock, mainly through farm-scale anaerobic digestion of manure from cattle and pigs	Agriculture
Intermittent aeration of continuously flooded rice paddies	
<b>BC 'Tech' measures<sup>4</sup> (affecting BC and other co-emitted compounds)</b>	
Diesel particle filters for road and off-road vehicles as part of a move to worldwide adoption of Euro 6/VI standards	Transport
Introduction of clean-burning biomass stoves for cooking and heating in developing countries <sup>2,3</sup>	Residential
Replacing traditional brick kilns with vertical shaft and Hoffman kilns	Industry
Replacing traditional coke ovens with modern recovery ovens, including the improvement of end-of-pipe abatement measures in developing countries	
<b>BC 'Reg' measures<sup>4</sup> (affecting BC and other co-emitted compounds)</b>	
Elimination of high-emitting vehicles in road and off-road transport	Transport
Ban on open burning of agricultural waste <sup>2</sup>	Agriculture
Substitution of clean-burning cookstoves using modern fuels (LPG or biogas) for traditional biomass cook stoves in developing countries <sup>2,3</sup>	Residential

<sup>1</sup>There are other measures than those identified that could be implemented. For example, a switch to electric vehicles would have a similar impact to diesel particulate filters but these have not been widely implemented yet; also forest fire controls could be important but are not included due to the difficulty in establishing the proportion of fires that are anthropogenic

<sup>2</sup>motivated in part by its effect on health and regional climate including areas of ice and snow

<sup>3</sup>For cook stoves, given their importance for BC emissions, two alternative measures are included

<sup>4</sup>The BC measures are grouped into those that are primarily technological (Tech) and those that are primarily regulatory (Reg)

Table S2. Average ratio of model to retrieved AERONET (AER) and Ozone Monitoring Instrument (OMI) clear-sky Aerosol Absorption Optical Depth at 550 nm within regions for the average of 14 AeroCom models and the two models used in the current study.

	AeroCom	GISS (2009)	MPIHAM (2009) [ECHAM]	GISS (this study)	ECHAM-HAMMOZ (this study)
AER, N Am #44	0.86	1.0	0.39	0.67	0.46
AER, Eur #41	0.81	0.83	0.21	0.67	0.28
AER, E Asia #11	0.67	0.49	0.29	0.50	0.31
AER, S Am #7	0.68	0.59	0.43	0.55	0.53
AER, SH Afr #5	0.53	0.35	0.35	0.39	0.61
AER, S/SE Asia #4	NA	NA	NA	0.43	0.47
AER, NH Afr #15	NA	NA	NA	1.22	0.45
OMI, N Am	0.52	0.73	0.21	0.70	0.49
OMI, Eur	1.6	1.4	0.29	0.91	0.41
OMI, E Asia	0.71	0.74	0.32	0.85	0.34
OMI, S Am	0.35	0.29	0.22	0.45	0.48
OMI, SH Afr	0.47	0.40	0.35	0.92	1.25
OMI, S/SE Asia	NA	NA	NA	0.85	1.07
OMI, NH Afr	NA	NA	NA	1.06	0.69

Number of measurement sites is given for AERONET, a network of ground-based aerosol lidars. Regions defined as NAm (130W to 70W; 20N to 55N), Europe (15W to 45E; 30N to 70N), E Asia (100E to 160E; 30N to 70N), SAm (85W to 40W; 34S to 2S), SH Afr (20W to 45E; 34S to 2S), S/SE Asia (60E to 110E; 10N to 30N), NH Afr (20W to 60E; 0 to 30N). AeroCom results and results from older versions of the two models used here (marked 2009) are from (18). The AERONET data are for 1996–2006, v2 level 2, and annual averages for each year were used if >8 months were present, and monthly averages for >10 days of measurements. The values at 550 nm were determined using the 0.44 and 0.87  $\mu\text{m}$  Angstrom parameters. Data from the OMI instrument on the NASA Aura satellite is based on OMAERUVd.003 daily products from 2005–2007 that were obtained through and averaged using NASA’s GIOVANNI system.

Table S3. Derivation of forcing values used in the temperature response calculations.

	Average forcing from GISS and ECHAM models	Forcing as a percentage of total anthropogenic forcing	Assessment range for anthropogenic forcing from literature	Resulting forcing used in temperature response calculation
CH <sub>4</sub> measures	O <sub>3</sub> : -.10 CH <sub>4</sub> : -.21 BC direct: .00 BC semi-direct +indirect: .00 BC dep: N/A OC: .00 SO <sub>4</sub> : -.02 SO <sub>4</sub> indirect: -.02 NO <sub>3</sub> : .00	-37% -44% 0% N/A 0% 0% 7% 7% 0%	O <sub>3</sub> : .35 (.25 to .45) CH <sub>4</sub> : .48 (.43 to .53) BC direct: .45 (.30 to .60) BC semi-direct +indirect: .00 (-.40 to .40) BC dep: .15 (.05 to .25) OC: -.20 (-.09 to -.31) SO <sub>4</sub> : -.29 (-.10 to -.48) SO <sub>4</sub> indirect: -.29 (-.10 to -.48) NO <sub>3</sub> : -.10 (-.03 to -.17)	O <sub>3</sub> : -.13 (-.09 to -.17) CH <sub>4</sub> : -.21 (-.19 to -.23) BC direct: .00 (.00 to .00) BC semi-direct +indirect: .00 (.00 to .00) BC dep: .00 (.00 to .00) OC: .00 (.00 to .00) SO <sub>4</sub> : -.02 (-.01 to -.03) SO <sub>4</sub> indirect: -.02 (-.01 to -.03) NO <sub>3</sub> : .00 (.00 to .00) Sum: -.38 (-.30 to -.46)
CH <sub>4</sub> + BC 'Tech' measures	O <sub>3</sub> : -.14 CH <sub>4</sub> : -.21 BC direct: -.10 BC semi-direct +indirect: .00 BC dep: N/A OC: .06 SO <sub>4</sub> : -.02 SO <sub>4</sub> indirect: -.02 NO <sub>3</sub> : .01	-52% -44% -31% N/A -38% -63% 7% 7% -10%		O <sub>3</sub> : -.18 (-.13 to -.23) CH <sub>4</sub> : -.21 (-.19 to -.23) BC direct: -.14 (-.09 to -.19) BC semi-direct +indirect: .00 (-.13 to .13) BC dep: -.06 (-.02 to -.10) OC: .13 (.06 to .20) SO <sub>4</sub> : -.02 (-.01 to -.03) SO <sub>4</sub> indirect: -.02 (-.01 to -.03) NO <sub>3</sub> : .01 (.00 to .02)

				Sum: -.49 (-.32 to -.66)
CH <sub>4</sub> + All BC measures	O <sub>3</sub> : -.15	-56%		O <sub>3</sub> : -.20 (-.14 to -.25)
	CH <sub>4</sub> : -.19	-40%		CH <sub>4</sub> : -.19 (-.17 to -.21)
	BC direct: -.21	-66%		BC direct: -.30 (-.20 to -.40)
	BC semi-direct +indirect: .00	N/A		BC semi-direct +indirect: .00 (-.26 to .26)
	BC dep: N/A	-66%		BC dep: -.10 (-.03 to -.17)
	OC: .07	-74%		OC: .15 (.07 to .23)
	SO <sub>4</sub> : -.02	7%		SO <sub>4</sub> : -.02 (-.01 to -.03)
	SO <sub>4</sub> indirect: -.02	7%		SO <sub>4</sub> indirect: -.02 (-.01 to -.03)
NO <sub>3</sub> : .01	10%		NO <sub>3</sub> : .01 (.00 to .02)	
				Sum: -.67 (-.23 to -1.10)

Notes: Radiative forcing due to BC deposition (called BC dep) was not calculated, rather BC deposition itself was used to derive the fractional change, which was multiplied by the assessed value of the effective forcing from BC deposition. The ECHAM model has more realistic internally mixed aerosols, so components are not separable, hence the relative contribution to aerosol forcing from individual species is based on the GISS model. The assessment range for anthropogenic forcing is not repeated for each measure as it is independent of measure.

Table S4. Regional response coefficients (C per W/m<sup>2</sup> local forcing)

Forcing region (x)	SHext	Tropics	NHml	Arctic	Global
Response region (a)					
SHext	0.19	0.05	0.02	0.00	0.39
Tropics	0.09	0.24	0.10	0.02	0.47
NHml	0.07	0.17	0.24	0.06	0.53
Arctic	0.06	0.16	0.17	0.31	0.64

Regional responses per unit forcing are the mean of responses to CO<sub>2</sub> and sulfate taken from Figure 1 of (55).

Table S5. Numerical values for the 10 top countries for each impact presented in Figure 4.

Avoided surface temperature increase ~2050 (C)		Decrease in atmospheric forcing (W/m <sup>2</sup> )	
<i>Country</i>	<i>Response</i>	<i>Country</i>	<i>Response</i>
Botswana	1.18	Bangladesh	10.6
Tajikistan	1.17	India	8.3
Kyrgyzstan	1.12	Bhutan	5.5
Russia	1.11	Nepal	5.3
Morocco	1.02	Togo	5.2
Algeria	1.01	Benin	5.1
Zimbabwe	1.00	Nigeria	4.8
Bulgaria	0.99	Ghana	4.7
Swaziland	0.96	Myanmar	4.7
Estonia	0.96	Rwanda	4.6
Annually avoided premature deaths		Annually avoided premature deaths per 100,000 people	
<i>Country</i>	<i>Response</i>	<i>Country</i>	<i>Response</i>
India	813566	Bangladesh	232
China	683592	Nepal	156
Bangladesh	159038	India	152
Pakistan	90593	Pakistan	137
Indonesia	89085	Uganda	125
Nigeria	69356	Nigeria	116
Viet Nam	58696	Viet Nam	114
Russia	39215	Rwanda	113
Ethiopia	24784	Bhutan	103
Nepal	24038	Congo	95
Annual tonnage crop production increase (white+rice+maize+soy)		Annual percentage crop yield increase (wheat+rice+maize+soy)	
<i>Country</i>	<i>Response</i>	<i>Country</i>	<i>Response</i>
China	15744000	Kuwait	8.0%
India	9775250	Iran	6.6%
United States	6305319	Jordan	6.5%
Pakistan	2134840	Israel	5.8%
Brazil	1640395	Pakistan	5.6%
Mexico	1135236	Armenia	4.8%
France	1123970	Lebanon	4.7%
Turkey	1043475	Malta	4.2%
Iran	1022335	Kyrgyzstan	4.2%
Egypt	948971	Mexico	4.1%

## References:

1. United Nations Environment Programme & World Meteorological Organization, “Integrated Assessment of Black Carbon and Tropospheric Ozone” (Nairobi, 2011).
2. W. Schopp, M. Amann, J. Cofala, C. Heyes, Z. Klimont, Integrated assessment of European air pollution emission control strategies. *Environ. Model. Softw.* **14**, 1 (1998).
3. M. Amann *et al.*, Cost-effective control of air quality and greenhouse gases in Europe: Modeling and policy applications. *Environ. Model. Softw.* **26**, 1489 (2011).
4. W. Tuinstra, Preparing for the European Thematic Strategy on air pollution: at the interface between science and policy. *Environmental Science & Policy* **10**, 434 (2007).
5. L. Hordijk, M. Amann, How science and policy combined to combat air pollution problems. *Environmental Policy and Law* **37**, 336 (2007).
6. M. Amann *et al.*, “GAINS-Asia. Scenarios for cost-effective control of air pollution and greenhouse gases in China” (IIASA Report, Laxenburg, Austria, 2008).
7. M. Amann *et al.*, “GAINS-Asia. Scenarios for cost-effective control of air pollution and greenhouse gases in India” (IIASA Report, Laxenburg, Austria, 2008).
8. J. G. J. Olivier, J. J. M. Berdowski, in *The Climate System*, J. Berdowski, R. Guicherit, B. J. Heij, Eds. (A.A. Balkema Publishers/Swets & Zeitlinger Publishers, Lisse, The Netherlands, 2001), pp. 33-78.
9. A. D. Jazcilevich *et al.*, An evaluation of the hybrid car technology for the Mexico Mega City *J. Power Sources* **196**, 5704 (2011).
10. M. A. Delucchi, M. Z. Jacobson, Providing all Global Energy with Wind, Water, and Solar Power, Part II: Reliability, System and Transmission Costs, and Policies. *Energy Policy* **39**, 1170 (2011).
11. D. T. Shindell *et al.*, Simulations of preindustrial, present-day, and 2100 conditions in the NASA GISS composition and climate model G-PUCCINI. *Atmos. Chem. Phys.* **6**, 4427 (2006).
12. D. Koch, G. Schmidt, C. Field, Sulfur, sea salt and radionuclide aerosols in GISS ModelE. *J. Geophys. Res.* **111**, D06206, doi:10.1029/2004JD005550 (2006).
13. D. Koch, J. Hansen, Distant origins of Arctic black carbon: A Goddard Institute for Space Studies ModelE experiment. *J. Geophys. Res.* **110**, D04204, doi:10.1029/2004JD005296 (2005).
14. S. E. Bauer *et al.*, Nitrate aerosols today and in 2030: importance relative to other aerosol species and tropospheric ozone. *Atmos. Chem. Phys.* **7**, 5043 (2007).
15. K. Tsigaridis, M. Kanakidou, Secondary organic aerosol importance in the future atmosphere. *Atmos. Environ.* **41**, 4682 (2007).
16. G. A. Schmidt *et al.*, Present day atmospheric simulations using GISS ModelE: Comparison to in-situ, satellite and reanalysis data. *J. Clim.* **19**, 153 (2006).
17. N. Butkovskaya, A. Kukui, G. Le Bras, HNO<sub>3</sub> Forming Channel of the HO<sub>2</sub> + NO Reaction as a Function of Pressure and Temperature in the Ranges of 72-600 Torr and 223-323 K *J. Phys. Chem. A* **111**, 9047 (2007).
18. D. Koch *et al.*, Evaluation of black carbon estimations in global aerosol models. *Atmos. Chem. Phys.* **9**, 9001 (2009).

19. A. M. Aghedo *et al.*, The vertical distribution of ozone instantaneous radiative forcing from satellite and chemistry climate models. *J. Geophys. Res.* **116**, D01305, doi:10.1029/2010JD014243 (2011).
20. D. T. Shindell *et al.*, Multi-model Projections of Climate Change From Short-lived Emissions Due To Human Activities. *J. Geophys. Res.* **113**, D11109, doi:10.1029/2007JD009152 (2008).
21. M. Schulz *et al.*, Radiative forcing by aerosols as derived from the AeroCom present-day and pre-industrial simulations. *Atmos. Chem. Phys.* **6**, 5225 (2006).
22. M. J. Prather, Numerical advection by conservation of second-order moments. *J. Geophys. Res.* **91**, 6671 (1986).
23. N. A. Rayner *et al.*, Global analyses of sea surface temperature, sea ice, and night marine air temperature since the late nineteenth century. *J. Geophys. Res.* **108**, doi 10.1029/2002JD002670 (2003).
24. L. Pozzoli *et al.*, Trace gas and aerosol interactions in the fully coupled model of aerosol-chemistry-climate ECHAM5-HAMMOZ: 1. Model description and insights from the spring 2001 TRACE-P experiment. *J. Geophys. Res.* **113**, D07308, (2008).
25. E. Roeckner *et al.*, Sensitivity of Simulated Climate to Horizontal and Vertical Resolution in the ECHAM5 Atmosphere Model. *J. Clim.* **19**, 3771 (2006).
26. S. Hagemann, K. Arpe, E. Roeckner, Evaluation of the Hydrological Cycle in the ECHAM5 Model. *J. Clim.* **19**, 3810 (2006).
27. S.-J. Lin, R. B. Rood, Multidimensional flux-form semi-Lagrangian transport schemes. *Mon. Weather Rev.* **124**, 2046 (1996).
28. L. W. Horowitz *et al.*, A global simulation of tropospheric ozone and related tracers: Description and evaluation of MOZART, version 2. *J. Geophys. Res.* **108**(D24), 4784, doi:10.1029/2002JD002853 (2003).
29. J. Feichter *et al.*, Simulation of the tropospheric sulfur cycle in a global climate model. *Atmos. Env.* **30**, 1693 (1996).
30. P. Stier *et al.*, The aerosol-climate model ECHAM5-HAM. *Atmos. Chem. Phys.* **5**, 1125 (2005).
31. E. Vignati, J. Wilson, P. Stier, M7: An efficient size-resolved aerosol microphysics module for large-scale aerosol transport models. *J. Geophys. Res.* **109**, D22202, (2004).
32. A. Guenther *et al.*, A global model of natural volatile organic compound emissions. *J. Geophys. Res.* **100**, 8873 (1995).
33. F. Dentener *et al.*, Emissions of primary aerosol and precursor gases in the years 2000 and 1750, prescribed data-sets for AeroCom. *Atmos. Chem. Phys.* **6**, 2703 (2006).
34. L. Pozzoli *et al.*, Trace gas and aerosol interactions in the fully coupled model of aerosol-chemistry-climate ECHAM5-HAMMOZ: 2. Impact of heterogeneous chemistry on the global aerosol distributions. *J. Geophys. Res.* **113**, D07309, (2008).
35. V. Ramaswamy *et al.*, in *Climate Change 2001*, J. T. Houghton, Ed. (Cambridge Univ. Press, Cambridge, 2001), pp. 349-416.
36. M. J. Prather *et al.*, in *Climate Change 2001*, J. T. Houghton, Ed. (Cambridge Univ. Press, Cambridge, 2001), pp. 239-287.
37. J. E. Penner *et al.*, Model intercomparison of indirect aerosol effects. *Atmos. Chem. Phys.* **6**, 3391 (2006).
38. M. M. Kvalevåg, G. Myhre, Human Impact on Direct and Diffuse Solar Radiation during the Industrial Era. *J. Clim.* **20**, 4874 (2007).

39. J. Quaas, O. Boucher, N. Bellouin, S. Kinne, Satellite-based estimate of the direct and indirect aerosol climate forcing. *J. Geophys. Res.* **113**, D05204, doi:10.1029/2007JD008962 (2008).
40. M. Christensen, G. Stephens, Microphysical and macrophysical responses of marine stratocumulus polluted by underlying ships: Evidence of cloud deepening. *J. Geophys. Res.* **116**, D03201, doi:10.1029/2010JD014638 (2011).
41. I. S. A. Isaksen *et al.*, Atmospheric composition change: Climate–Chemistry interactions. *Atmos. Env.* **43**, 5138 (2009).
42. V. Ramanathan, G. Carmichael, Global and regional climate changes due to black carbon. *Nature Geosci.* **1**, 221 (2008).
43. P. Forster *et al.*, in *Climate Change 2007: The Physical Science Basis*, S. Solomon, Ed. (Cambridge University Press, New York, 2007).
44. M. Sato *et al.*, Global atmospheric black carbon inferred from AERONET. *Proc. Natl. Acad. Sci.* **100**, 6319 (2003).
45. D. Koch, A. Del Genio, Black carbon semi-direct effects on cloud cover: review and synthesis. *Atmos. Chem. Phys.* **10**, 7685 (2010).
46. W. T. Chen, Y. H. Lee, P. J. Adams, A. Nenes, J. H. Seinfeld, Will black carbon mitigation dampen aerosol indirect forcing? *Geophys. Res. Lett.* **37**, L09801, 10.1029/2010GL042886 (2010).
47. J. R. Pierce, P. J. Adams, Uncertainty in global CCN concentrations from uncertain aerosol nucleation and primary emission rates. *Atmos. Chem. Phys.* **9**, 1339 (2009).
48. X. Liu *et al.*, Uncertainties in global aerosol simulations: Assessment using three meteorological datasets. *J. Geophys. Res.* **112**, D11212, doi:10.1029/2006JD008216 (2007).
49. S. G. Warren, W. J. Wiscombe, A Model for the Spectral Albedo of Snow. II: Snow Containing Atmospheric Aerosols. *J. Atmos. Sci.* **37**, 2734 (1980).
50. M. G. Flanner, C. S. Zender, J. T. Randerson, P. J. Rasch, Present-day climate forcing and response from black carbon in snow. *J. Geophys. Res.* **112**, D11202, doi:10.1029/2006JD008003 (2007).
51. D. Koch *et al.*, Distinguishing aerosol impacts on climate over the past century. *J. Climate* **22**, 2659 (2009).
52. G. Myhre, Consistency Between Satellite-Derived and Modeled Estimates of the Direct Aerosol Effect. *Science* **325**, 187 (2009).
53. D. M. Murphy *et al.*, An observationally based energy balance for the Earth since 1950. *J. Geophys. Res.* **114**, D17107, doi:10.1029/2009JD012105 (2009).
54. N. Bellouin, A. Jones, J. Haywood, S. A. Christopher, Updated estimate of aerosol direct radiative forcing from satellite observations and comparison against the Hadley Centre climate model. *J. Geophys. Res.* **113**, doi:10.1029/2007JD009385 (2008).
55. D. Shindell, G. Faluvegi, Climate response to regional radiative forcing during the 20th century. *Nature Geosci.* **2**, 294 (2009).
56. C. E. Chung, V. Ramanathan, D. Kim, I. A. Podgorny, Global anthropogenic aerosol direct forcing derived from satellite and ground-based observations. *J. Geophys. Res.* **110**, D24207, doi:10.1029/2005JD006356 (2005).
57. U. Siegenthaler, F. Joos, Use of a simple model for studying oceanic tracer distributions and the global carbon cycle. *Tellus* **44**, 186 (1992).

58. G. Marland, T. A. Boden, R. J. Andres, *Global, Regional, and National Fossil Fuel CO<sub>2</sub> Emissions, in Trends: A Compendium of Data on Global Change*. (Carbon Dioxide Information Analysis Center, Oak Ridge National Laboratory, U.S. Department of Energy, Oak Ridge, 2008).
59. K. P. Shine, J. S. Fuglestvedt, K. Hailemariam, N. Stuber, Alternatives to the Global Warming Potential for Comparing Climate Impacts of Emissions of Greenhouse Gases. *Clim. Change* **68**, 281 (2005).
60. D. Shindell, G. Faluvegi, The net climate impact of coal-fired power plant emissions. *Atmos. Chem. Phys.* **10**, 3247 (2010).
61. O. Boucher, P. Friedlingstein, B. Collins, K. P. Shine, The indirect global warming potential and global temperature change potential due to methane oxidation. *Environ. Res. Lett.* **4**, doi:10.1088/1748 (2009).
62. O. Boucher, M. S. Reddy, Climate trade-off between black carbon and carbon dioxide emissions. *Energy Policy* **36**, 193 (2008).
63. J. Hansen *et al.*, Efficacy of Climate Forcings. *J. Geophys. Res.* **110**, **D18104**, doi:10.1029/2005JD005776 (2005).
64. D. S. Stevenson *et al.*, Multi-model ensemble simulations of present-day and near-future tropospheric ozone. *J. Geophys. Res.* **111**, **D08301**, doi:10.1029/2005JD006338 (2006).
65. G. C. Hegerl *et al.*, in *Intergovernmental Panel on Climate Change Fourth Assessment Report*, S. Solomon, Ed. (Cambridge, New York, 2007).
66. J. Hansen *et al.*, A closer look at United States and global surface temperature change. *J. Geophys. Res.* **106**, 23947 (2001).
67. T. C. Bond *et al.*, Historical emissions of black and organic carbon aerosol from energy-related combustion, 1850–2000. *Global Biogeochem. Cycles* **21**, **GB2018**, doi:10.1029/2006GB002840 (2007).
68. R. Van Dingenen *et al.*, The global impact of ozone on agricultural crop yields under current and future air quality legislation. *Atmos. Env.* **43**, 604 (2009).
69. K. Aunan, T. K. Berntsen, H. M. Seip, Surface ozone in China and its possible impact on agricultural crop yields. *Ambio* **29**, 294 (2000).
70. G. Fischer, H. van Velthuisen, F. Nachtergaele, S. Medow, “Global Agro-Ecological Zones (Global - AEZ)” (Food and Agricultural Organization/International Institute for Applied Systems Analysis, 2000).
71. Z. Feng, K. Kobayashi, Assessing the impacts of current and future concentrations of surface ozone on crop yield with meta-analysis. *Atmos. Env.* **43**, 1510 (2009).
72. D. Shindell *et al.*, Climate, health, agricultural and economic impacts of tighter vehicle-emission standards. *Nature Climate Change* **1**, 59 (2011).
73. D. Krewski *et al.*, “Extended follow-up and spatial analysis of the American Cancer Society study linking particulate air pollution and mortality” (Health Effects Institute, 2009).
74. M. Jerrett *et al.*, Long-Term Ozone Exposure and Mortality. *New Engl. J. Med.* **360**, 1085 (2009).
75. C. A. Pope *et al.*, Lung cancer, cardiopulmonary mortality, and long-term exposure to fine particulate air pollution. *JAMA* **287**, 1132 (2002).
76. H. A. Roman *et al.*, Expert judgment assessment of the mortality impact of changes in ambient fine particulate matter in the US. *Environ. Sci. Technol.* **42**, 2268 (2008).

77. N. Nakicenovic *et al.*, *IPCC Special Report on Emissions Scenarios*. (Cambridge University Press, Cambridge, UK, 2000), pp. 570.
78. S. C. Anenberg, L. W. Horowitz, D. Q. Tong, J. J. West, An estimate of the global burden of anthropogenic ozone and fine particulate matter on premature human mortality using atmospheric modeling. *Environ. Health Perspect.* **118**, 1189 (2010).
79. K. R. Smith, J. L. Peel, Mind the Gap. *Environ. Health Perspect.* **118**, (2010).
80. C. A. Pope III *et al.*, Cardiovascular mortality and exposure to airborne fine particulate matter and cigarette smoke: shape of the exposure-response relationship. *Circulation* **120**, 941 (2009).
81. K. R. Smith *et al.*, Public health benefits of strategies to reduce greenhouse-gas emissions: health implications of short-lived greenhouse pollutants. *The Lancet* **374**, 2091 (2009).
82. M. L. Bell, K. Ebisu, R. D. Peng, J. M. Samet, F. Dominici, Hospital admissions and chemical composition of fine particle air pollution. *American Journal of Respiratory and Critical Care Medicine* **179**, 1115 (2009).
83. H. R. Anderson, R. W. Atkinson, J. L. Peacock, L. Marston, K. Konstantinou, "Meta-analysis of time-series studies and panel studies of particulate matter (PM) and ozone (O<sub>3</sub>)" (World Health Organization, Copenhagen, 2004).
84. "Public Health and Air Pollution in Asia (PAPA): Coordinated Studies of Short-Term Exposure to Air Pollution and Daily Mortality in Four Cities" (Health Effects Institute, Boston, 2010).
85. World Health Organisation, "Comparative Quantification of Health Risks: Global and Regional Burden of Disease (specifically Chapter 18 Indoor Air Pollution from Household Use of Solid Fuels. Kirk R Smith, Sumi Mehta, Mirjam Maeusezahl-Feuz)" (WHO, Geneva, 2004).
86. M. L. Cropper, W. E. Oates, Environmental Economics: A Survey. *J. Econ. Lit.* **30**, 675 (1992).
87. W. K. Viscusi, J. E. Aldy, The Value of a Statistical Life: A Critical Review of Market Estimates Throughout the World. *J. Risk Uncert.* **27**, 5 (2003).
88. USEPA, "The Benefits and Costs of the Clean Air Act: 1990 - 2010. EPA Report to Congress" (Office of Air and Radiation, Office of Policy, Washington, DC, 1999).
89. World\_Bank, <http://databank.worldbank.org/ddp>. (2010).
90. L. Höglund-Isaksson, W. Winiwarter, A. Tohka, "Potentials and costs for mitigation of non-CO<sub>2</sub> greenhouse gases in the European Union until 2030 - Methodology" (IIASA Report, 2010).
91. L. Höglund-Isaksson, W. Winiwarter, F. Wagner, Z. Klimont, M. Amann, "Potentials and costs for mitigation of non-CO<sub>2</sub> greenhouse gases in the European Union until 2030" (IIASA Report, 2010).